

Probing quadratic gravity with black-hole ringdown gravitational waves measured by LIGO-Virgo-KAGRA detectors

Adrian Ka-Wai Chung^{1,*} and Nicolás Yunes¹

¹*Illinois Center for Advanced Studies of the Universe & Department of Physics,
University of Illinois Urbana-Champaign, Urbana, Illinois 61801, USA*

(Dated: June 18, 2025)

quadratic-gravity theories emerge as the low-energy limit of many grand-unified and quantum-gravity theories. We report the first gravitational-wave ringdown constraints on such theories obtained purely from the quasinormal-mode spectra of rapidly-spinning black-hole remnants. We find no quadratic-gravity signatures from ringdown signals measured by the LIGO-Virgo-KAGRA detectors, thereby constraining the coupling length scale of axi-dilaton gravity below 34 km, dynamical Chern-Simons gravity below 49 km, and scalar Gauss-Bonnet gravity below 47 km.

Introduction. The nature of gravity remains one of the most profound open questions in fundamental physics. Although general relativity has withstood a century of tests and it remains the most accurate theory of gravity [1], it is recognized to be incomplete, as it is notably incompatible with quantum mechanics at microscopic scales [2]. Beyond this theoretical limitation, general relativity struggles to explain some astrophysical phenomena, such as the late-time acceleration of the Universe [3, 4], and galaxy rotation curves [5, 6], without invoking dark matter and dark energy. These challenges have motivated a wide range of extensions to general relativity.

To identify viable extensions, we must examine their consistency with experimental and observational data. Gravitational waves offer a powerful avenue for such tests. Most of the gravitational waves that have been detected so far have been produced from black hole mergers [7–9], a natural laboratory to probe gravity in the strong and highly non-linear regime [10–12]. In this regime, any deviations from general relativity would manifest in the dynamics of spacetime and the gravitational-wave signals emitted. Thus, by comparing observed signals with theoretical predictions, we can either detect signs of new physics or place stringent constraints on violations of general relativity.

Gravitational waves from the ringdown of black hole mergers are especially well-suited for testing general relativity. In this phase, the newly formed, perturbed black hole settles into its final stationary state by emitting gravitational waves, composed of exponentially damped sinusoids. The frequencies and decay times of these waves, called quasinormal modes, are determined solely by the spacetime around the remnant black hole, and they largely shape the ringdown waveform. As noted in [13], ringdown waves typically have the highest frequencies in the signal, corresponding to the most rapidly-varying spacetime dynamics, which can reveal deviations from general relativity hidden in other phases. Furthermore, quasinormal modes probe the near-horizon region of spacetime, where gravitational fields are the strongest and general relativity

may be most likely to break down. These features make the ringdown phase a powerful probe of the nature of gravity in the strong-field regime [14].

To extract physics from ringdown tests, we must first know the quasinormal-mode spectra of black holes when general relativity is modified in specific ways. This presents a formidable mathematical challenge, as it requires solving a system of highly-coupled and lengthy partial differential equations that governs the perturbations of rotating black holes. Consequently, almost all current ringdown tests of general relativity have been either model-agnostic, or limited to specific extensions that rely heavily on the small-spin approximation to model quasinormal-mode spectra, which biases the analyses. Recently, the development of the *Metric pErTuRbations wIth speCtral methodS* (METRICS) framework [13, 15–17] and the modified Teukolsky formalism [18–23] have enabled, for the first time, to accurately compute quasinormal-mode spectra for black holes beyond general relativity with the (moderate and large) spins relevant to gravitational-wave observations. With these spectra, we can perform robust and accurate ringdown tests targeted at these extensions.

In this work, we present the first robust and accurate ringdown tests of quadratic-gravity theories by applying recently computed quasinormal-mode spectra from the METRICS code to black-hole ringdown signals detected by the LIGO-Virgo-KAGRA detectors. We focus on three well-motivated extensions of general relativity: axi-dilaton gravity, dynamical Chern-Simons gravity, and scalar-Gauss-Bonnet gravity. These theories naturally emerge in the low-energy limits of grand unified frameworks, such as string theory [24], or quantum-gravity candidates, like loop quantum gravity [25]. Axi-dilaton gravity also offers a possible mechanism for cosmological inflation [26], while the parity-violating nature of dynamical Chern-Simons gravity offers a possible explanation to baryon asymmetry [27].

Our analyses significantly improve upon previous gravitational-wave tests of these theories. First, we use QNM spectra accurate for spinning black holes with dimensionless spin $a = |\vec{J}|/M^2 \in [0, 0.75]$, encompassing the spin range of most remnant black holes observed by LIGO-Virgo-KAGRA; previous analyses typically relied on first-

* akwchung@illinois.edu

order-in-spin approximations. Second, our analysis addresses the splitting of the quasinormal-mode spectra of axial and polar metric perturbations, whereas earlier analyses considered only the least-damped or dominant-parity mode. These improvements make our tests more complete, precise and robust. Finding no quadratic-gravity signature, we place new bounds on these quadratic-gravity theories, including the first gravitational-wave constraints on axi-dilaton gravity. Given the central role these theories play in fundamental physics today, our results offer valuable insights across high-energy theory, quantum gravity, and early-Universe cosmology.

Quadratic gravity. The Lagrangian density of quadratic gravity involves at most the quadratic product of curvature quantities, such as the Riemann tensor $R_{\mu\nu\rho\sigma}$ (or its dual ${}^*R^{\mu\nu\rho\sigma}$), the Ricci tensor $R_{\mu\nu}$ and the Ricci scalar R . The Lagrangian density of these theories can be compactly written as [24]

$$16\pi\mathcal{L} = R + \alpha_1\varphi_1\mathcal{G} + \alpha_2(\varphi_1\sin\theta_m + \varphi_2\cos\theta_m)\mathcal{P} - \frac{1}{2}\nabla_\mu\varphi_1\nabla^\mu\varphi_1 - \frac{1}{2}\nabla_\mu\varphi_2\nabla^\mu\varphi_2, \quad (1)$$

where $\alpha_{1,2}$ are coupling constants of quadratic gravity, which have the dimension of length squared, φ_1 (φ_2) is a scalar (pseudo-scalar) field to which the black hole couples, $\mathcal{G} = R^2 - 4R_{\alpha\beta}R^{\alpha\beta} + R_{\alpha\beta\gamma\delta}R^{\alpha\beta\gamma\delta}$ is the Gauss-Bonnet invariant [28], $\mathcal{P} = R_{\mu\nu\rho\sigma}{}^*R^{\mu\nu\rho\sigma}$ is the Pontryagin invariant [25], and θ_m is the mixing angle, which characterizes the relative composition of the Lagrangian in terms of \mathcal{G} and \mathcal{P} . This Lagrangian density reduces to scalar-Gauss-Bonnet gravity when $\alpha_2 = 0$ and $\alpha_1 := \ell_{\text{sGB}}^2$, to dynamical Chern-Simons gravity when $\alpha_1 = 0$, $\theta_m = 0$, and $\alpha_2 := \ell_{\text{CS}}^2$, and to axi-dilaton gravity when $\alpha_1 = \alpha_2 := \ell_{\text{AD}}^2$ and $\theta_m = 0$. The parameter ℓ , which can be ℓ_{sGB} , ℓ_{CS} , or ℓ_{AD} , characterizes the effective coupling length scales of the respective quadratic-gravity theories. A more general form of the coupling functions (the coefficient of \mathcal{G} and \mathcal{P}) can, in principle, be considered. In this work, we focus on the chosen form because it serves as the leading-order approximation of more complex coupling functions in the regime where $\alpha_{1,2}$ and $|\varphi_{1,2}|$ are small. This is a justified assumption given that general relativity has passed all tests.

Waveform model. Gravitational waves emitted by a remnant black hole during its ringdown phase can be well described by [29]

$$h(t) = \frac{M_z}{d_L}\Theta(t-t_s)\sum_{n,l,m,q}S_{nlm}(\iota,\phi)\left[A_{nlm}^{P,q}e^{-i\omega_{nlm}^q(t-t_s)} + A_{nlm}^{N,q}e^{-i(\omega_{nlm}^q)^\dagger(t-t_s)}\right], \quad (2)$$

where $\sum_{n,l,m,q}$ stands for summation over $n \geq 0, l \geq 2, -l \leq m \leq l$, while $q = \text{axi}$ (the axial modes) or $q = \text{pol}$ (the polar modes), M_z is the (redshifted) remnant mass in the detector frame, d_L is the luminosity distance to the

remnant black hole, and $\Theta(t-t_s)$ is a Heaviside function that activates the waveform at the ringdown start time t_s . The quantity $S_{nlm}(\iota,\phi)$ are spin-weighted spheroidal harmonics, which are functions of the angle ι between the remnant spin axis and the line of sight, and the azimuthal angle ϕ in the line of sight in the source frame.

The quantity ω_{nlm}^q in the waveform of Eq. (2) are (complex) quasinormal-mode frequencies. For astrophysical black holes in general relativity, ω_{nlm}^q depends only on the remnant mass M_z and dimensionless spin a^1 [31], and is independent of q due to isospectrality [32, 33]. In quadratic gravity, ω_{nlm}^q also depends on the effective coupling length scale ℓ . Since general relativity has passed all experimental and observational tests to date, we expect deviations from general relativity, if present, to be small, which implies ℓ should also be small. In this small-coupling limit, ω_{nlm}^q can be expressed as

$$\omega_{nlm}^q(M_z, a, \ell) = \omega_{nlm}^{q,(0)}(M_z, a) + \frac{\zeta}{M_z}\omega_{nlm}^{q,(1)}(a), \quad (3)$$

where $\omega_{nlm}^{q,(0)}$ are the quasinormal-mode frequencies in general relativity, we have introduced the dimensionless coupling parameter

$$\zeta = \left[\frac{\ell(1+z)}{M_z}\right]^4, \quad (4)$$

z is the redshift to the remnant black hole because M_z is redshifted, and $\omega_{nlm}^{q,(1)}$ is the leading-order frequency shift in ζ . The quadratic-gravity correction $\omega_{nlm}^{q,(1)}$ of dynamical Chern-Simons and scalar Gauss-Bonnet gravity are known to be accurate for spins $a \lesssim 0.75$ in the METRICS framework [13, 16, 17]. In the Supp. Mat., we show that $\omega_{nlm}^{q,(1)}$ in axi-dilaton gravity is just the summation of that of dynamical Chern-Simons and scalar-Gauss-Bonnet gravity. In this work, we use the fitting expressions for $\omega_{nlm}^{q,(1)}$ provided in [13, 16, 17] for our tests of quadratic-gravity theories. Although in parameter estimation we occasionally need to explore spins $a > 0.75$, where the METRICS $\omega_{nlm}^{q,(1)}$ have not been accurately computed yet, we will show here that our posteriors have most of their support inside $a \leq 0.75$ (see Supp. Mat.).

The quantities $A_{nlm}^{P,q}$ and $A_{nlm}^{N,q}$ are complex mode amplitudes. The superscript P (N) stands for modes with a positive (negative) real-part frequency. For non-precessing binary black holes in gravity theories that respect parity symmetry, such as scalar Gauss-Bonnet gravity, the mode amplitudes satisfy the relation $A_{nlm}^{N,q} = (-1)^l(A_{nlm}^{P,q})^\dagger$ [29]. In our analysis, we assume this relation also holds in the other two gravity theories considered here, whose

¹ Strictly speaking, ω_{nlm}^q in general relativity can also depend on electric charge. However, any electric charge carried by astrophysical black holes is expected to be neutralized quickly by the astrophysical environment [30].

Lagrangians include the parity-violating Pontryagin density. This assumption is justified on two grounds. First, the corrections to the mode amplitudes, and thus the deviation from the relation $A_{nlm}^{N,q} = (-1)^l (A_{nlm}^{P,q})^\dagger$, due to quadratic-curvature couplings are of $\mathcal{O}(\zeta)$, which is the same order as the shift in the quasinormal-mode frequencies. However, current ground-based detectors are much more sensitive to the gravitational-wave phase than their amplitude [34], and thus, it is reasonable to neglect modifications to the latter. Second, any change to the mode amplitude is an additional observable signature that would strengthen constraints on quadratic-gravity theories. Neglecting such changes leads a conservative test. By similar reasoning, we also omit the scalar-led quasinormal modes, as their amplitude is of $\mathcal{O}(\zeta)$.

Bayesian inference framework. The goal of this work is to constrain the parameter ℓ in various quadratic-gravity theories using detected ringdown signals via Bayesian inference. We construct the marginalized posterior

$$p(\ell|d, H, I) = \int d\vec{\theta} p(\ell, \vec{\theta}|d, H, I), \quad (5)$$

where $\vec{\theta}$ denotes other source parameters (e.g., M_z and d_L), d is the strain data, H is the hypothesis that the signal includes quadratic-gravity effects, and I encodes prior knowledge, such as the quasinormal-mode spectra. By Bayes' theorem,

$$p(\ell, \vec{\theta}|d, H, I) = \frac{p(d|\ell, \vec{\theta}, H, I)p(\ell, \vec{\theta}|H, I)}{p(d|H, I)}, \quad (6)$$

where $p(d|\ell, \vec{\theta}, H, I)$ is the likelihood, $p(\ell, \vec{\theta}|H, I)$ is the prior, and $p(d|H, I)$ is the evidence. If multiple events are analysed, $d = \{d_i|i = 1, 2, 3, \dots\}$, where d_i is the data of the i -th event, the combined posterior is

$$p(\ell|d, H, I) \propto \prod_{i=1} p(\ell|d_i, H, I), \quad (7)$$

since ℓ is a coupling constant and the prior of ℓ is uniform (see the next section), which is the same in different events. The 90%-confidence interval ℓ_{90} , defined by

$$\int_0^{\ell_{90}} d\ell p(\ell|d, H, I) = 0.9, \quad (8)$$

gives us constraints on quadratic-gravity theories.

Parameter estimation. We analyze LIGO-Virgo-KAGRA open data and focus on the events whose ringdown signals have been subjected to LIGO-Virgo-KAGRA ringdown-alone tests of general relativity in [11, 12]. Since the resulting posterior on ℓ is expected to be dominated by the most stringent individual constraints, we concentrate on those ringdown signals with the largest signal-to-noise ratio, namely, GW150914 [7], GW190521-074359 [8], and GW200129-065458 [9]. The progenitor binaries of these events exhibit no significant spin precession [9, 35], consistent with the symmetry assumption used to derive

$A_{nlm}^{N,q} = (-1)^l (A_{nlm}^{P,q})^\dagger$ in Eq. (2). While there is some evidence the detected ringdown signals may contain overtone(s) [36, 37], we include only the $nlm = 022$ mode in our analysis; adding an overtone does not significantly impact our results (see Supp. Mat.).

We analyze the ringdown signals using `pyRing` [38], a Python package for time-domain black-hole spectroscopy [39–41]. To avoid contamination from nonlinear effects present during the merger phase [42, 43], we begin our analysis at a time $10M_z$ after the peak of the strain amplitude. Both the peak time and the total mass M_z can be estimated *a priori* by analyzing the full gravitational-wave signal assuming general relativity, and these values are available from the data release accompanying [11]. Following standard procedures in black-hole spectroscopy [11, 12, 29], we fix the sky location to the maximum-likelihood value obtained from full-signal parameter estimation; this is legitimate, as modifications from quadratic gravity do not affect the inferred sky position or luminosity distance. We prescribe a uniform prior on the following parameters, following [29]: $M_z \in [10, 500] M_\odot$, $a \in [0, 0.93]$, $|A_{nlm}^{P/N,q}| \in [0, 50]$, and $\phi_{nlm}^{P/N,q} = \arg(A_{nlm}^{P/N,q}) \in [0, 2\pi]$. For the luminosity distance d_L , we use uniform priors bounded by the 95% credible interval of the posterior distribution reported by the LIGO-Virgo-KAGRA collaborations. The redshift is related to d_L through the linear approximation $z = H_0 d_L$, where $H_0 = 67.9 \text{ km s}^{-1} \text{ Mpc}^{-1}$ is the Planck 2015 value of the Hubble constant [44]. This is a good approximation for the low-redshift sources considered in our analysis. The prior of ℓ is uniform in $[0, 500] \text{ km}$. However, to ensure consistency with the small-coupling approximation and to avoid unphysical waveforms (e.g. with exponentially-growing ringdown amplitudes), we exclude values of ℓ corresponding to $\zeta > 1$ or $\text{Im}(\omega) \geq 0$. The posteriors are sampled with 4096 live points and we estimate the posterior using a kernel density estimator. We have checked that our results are robust to the starting time of the ringdown analysis, the prior used on the astrophysical parameters, and the small-coupling approximation, as we show below.

Analysis of LIGO-Virgo-KAGRA ringdown data. The left, middle, and right panels of Fig. 1 show the posteriors of ℓ for axi-dilaton, dynamical Chern-Simons, and scalar Gauss-Bonnet gravity theories, respectively, obtained by analyzing the ringdown phase of GW150914 (dashed blue), GW190521-074359 (dash-dotted red), and GW200129-065458 (dotted green), along with the combined posterior (solid black). For $\ell \lesssim 30\text{--}60 \text{ km}$, a range comparable to the remnant black hole masses, the posteriors have relatively large and nearly constant support. Beyond this range, the posteriors rapidly decline to nearly zero, as expected if general relativity is correct. When $\ell \lesssim M$, the frequency shifts in the quasinormal modes induced by quadratic-gravity corrections remain within the uncertainties of the observed ringdown signals and are therefore not ruled out. However, as ℓ increases, these frequency shifts become more significant and are no longer

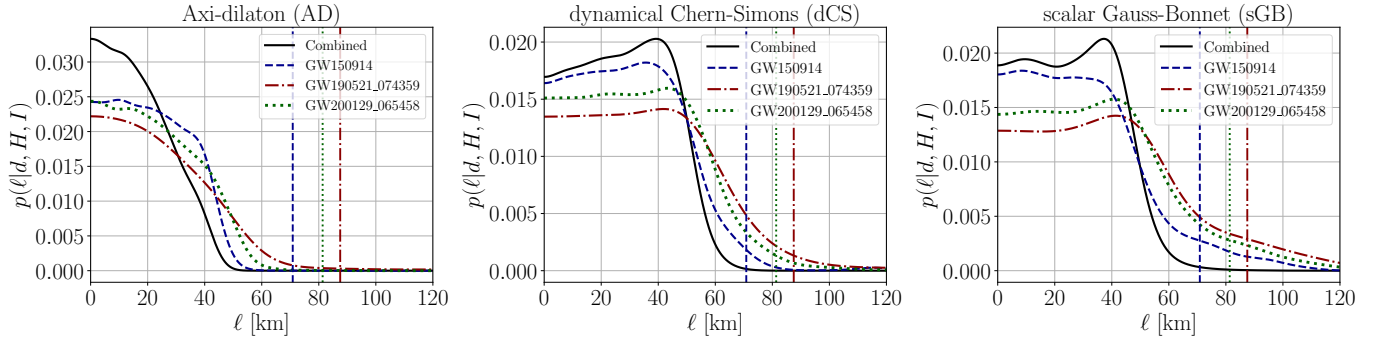


FIG. 1. The marginalized posterior of ℓ (in km) for axi-dilaton (left), dynamical Chern-Simons (middle), and scalar Gauss-Bonnet (right) gravity obtained by analyzing the ringdown signal of GW150914 (dashed blue), GW190521_074359 (dash-dotted red), and GW200129_065458 (dotted green), and the combined posterior (solid black). The vertical line of matching style indicates the maximum allowed $\ell := M_{\text{map}}^{1/4}$ within the small-coupling approximation for the corresponding signal, where M_{map} is the maximal-posterior remnant mass inferred assuming general relativity.

consistent with the data, and are thus excluded by the data. As all posteriors are consistent with $\ell = 0$, we conclude that no quadratic-gravity signatures are detected from the ringdown signals. By numerically solving Eq. (2), we estimate the 90% confidence interval, ℓ_{90} , for each theory. These constraints are summarized in Table I, which includes the first constraint ever on axi-dilaton gravity.

Observe that the posteriors for ℓ in axi-dilaton gravity are the most narrow, with a tighter 90%-confidence interval, compared to the other quadratic-gravity theories. This feature is reasonable because the shift of the quasinormal-mode frequencies in axi-dilaton gravity is the sum of that in dynamical Chern-Simons and scalar Gauss-Bonnet gravity. In the former, axial quasinormal-mode spectra are more significantly modified, while in the latter, stronger modifications appear in the polar spectra. Consequently, axi-dilaton coupling modifies both parity sectors manifestly, making it an easier theory to rule out and leading to the most stringent constraints on ℓ .

Robustness checks. We have verified that our results are robust and consistent with the assumptions underlying our analysis. First, we have confirmed that all posterior samples satisfy $\zeta \ll 1$, ensuring that the small-coupling approximation remains valid. We have also verified that our constraints on ℓ are not artifacts of excluding $\zeta \geq 1$ or $\text{Im}(\omega) > 0$ from the priors. The width of the ℓ posteriors in dynamical Chern-Simons gravity agrees with previous estimates [17], further supporting the validity of our inference. We also find no significant degeneracy between ℓ and the remnant black hole's mass and spin (i.e., a waveform with nonzero ℓ cannot mimic a general-relativity waveform with different M_z and a). Additionally, we have confirmed that relaxing the approximation $A_{nlm}^{N,q} = (-1)^l (A_{nlm}^{P,q})^\dagger$ and including an overtone do not significantly affect the constraints. Finally, we have checked that our results are robust against numerical errors in the METRICS computations, systematic errors in the quasinormal-mode spectra model for spins $a > 0.75$, and the choice of ring-

down start time, provided that merger nonlinearities have sufficiently subsided. All checks are detailed in Supp. Mat.

Comparison with other analyses. This work is the first to constrain quadratic gravity from ringdown signals alone, but one other work has considered tests of cubic gravity [29], a theory that does not include scalar fields. The widths and ℓ_{90} values of the posteriors we found for quadratic-gravity theories are comparable to those found for cubic gravity [29]. This numerical coincidence can be understood physically by considering dynamical Chern-Simons gravity (though similar reasoning applies more generally) as follows. The scalar field φ_2 obeys $\square \varphi_2 + \alpha_2 \mathcal{P} = 0$, where \square is the d'Alembertian operator, and thus, $\varphi_2 = -\alpha_2 \square^{-1} \mathcal{P}$. Heuristically, given a characteristic length scale λ , the curvature scales as λ^{-2} , so $\mathcal{P} \sim \lambda^{-4}$ and $\square^{-1} \sim \lambda^2$, yielding $\varphi_2 \sim \lambda^{-2}$. The dynamical Chern-Simons corrections to the Lagrangian, $\alpha_2 \varphi_2 \mathcal{P}$ and $\partial_\mu \varphi_2 \partial^\mu \varphi_2$, then scale as λ^{-6} , roughly cubic in curvature scale, as is also the case in cubic gravity theories. This explains why our constraints on quadratic gravity are similar to those on cubic theories. Note also that the $nlm = 122$ is included in [29] but omitted here. The agreement between results also confirms that the inclusion of additional modes does not significantly affect the constraints.

Our constraints on quadratic gravity differ from those in [45] by a factor of ~ 4 because of various differences in analysis methodology. First, [45] included the inspiral, merger and ringdown phases in their analysis, with quadratic-gravity changes only in the merger and ringdown phase (even though modifications to the merger are not known accurately), while we only consider the ringdown phase. Their whole-signal analysis recovers a signal-to-noise ratio of ~ 25 , whereas our ringdown-only analysis yields signal-to-noise ratios $\lesssim 7$, roughly a factor of 4 smaller. Second, their analyses uses a model for the quasinormal-mode frequency shift that is accurate only to first order in a , which is valid when $a \lesssim 0.3$, while

90 % interval on ℓ [km]	GW150914	GW190521.074359	GW200129.065458	Combined
Gravity theories				
Axi-dilaton (AD)	39.8	55.9	43.8	33.9
dynamical Chern-Simons (dCS)	53.6	75.9	61.1	48.5
scalar Gauss-Bonnet (sGB)	46.5	57.5	83.4	46.5

TABLE I. The 90% confidence intervals on ℓ , as defined in Eq. (8), for various quadratic-gravity theories. The constraints are obtained by analyzing the ringdown signals of GW150914, GW190521.074359, and GW200129.065458 individually, as well as from their combined posterior.

our analysis uses the METRICS model, which is accurate up to $a \lesssim 0.75$ and thus applicable to black-hole remnants produced in the collision of non-spinning black holes. Third, their analysis includes only the less-damped parity sector of each theory, whereas we incorporate shifts in both axial and polar quasinormal modes. Therefore, although the reported constraints in [45] are more stringent (due to the use of a larger signal-to-noise ratio), the results presented here are more robust.

Concluding remarks. Our work advances the understanding of potential violations of fundamental physics by providing accurate modeling and robust analysis of gravitational waves emitted by black holes and observed by the LIGO–Virgo–KAGRA detectors. Notably, we report the first observational constraint on axi-dilaton gravity, a theory that arises in the low-energy limit of string theory and offers a plausible mechanism for cosmological inflation. Our results also constrain violations of key principles underlying general relativity, including the strong equivalence principle (via the presence of scalar fields), parity symmetry in gravity, and the assumption that gravity is fully described by a metric tensor. These findings provide valuable insights for the development of theoretical models aimed at explaining the early Universe, grand unification, and physics beyond the Standard Model. While some of our constraints are less stringent than some previous analyses, our work (i) probes a complementary dynamical regime, black hole ringdown, where near-horizon physics is at play, and (ii) employs a more robust methodology, accounting for the breaking of isospectrality and using a quasinormal-mode spectra model that is accurate and precise for moderate to large spins.

Our work marks a major step toward physics-informed tests of general relativity using gravitational-wave observations. Looking ahead, we aim to incorporate the accurate quasinormal-mode spectra into a comprehensive waveform model that accounts for isospectrality breaking, along with modifications to the inspiral and ringdown phases, and the merger time. Such a model will enable more precise and self-consistent tests of alternative gravity theories. Future efforts could also focus on computing corrections to waveform amplitude and polarization content due to quadratic-gravity couplings, and incorporating scalar-branch quasinormal modes, further enhancing the accuracy of these tests. These developments will expand the toolkit for extracting fundamental physics from gravitational-wave data, fully preparing us to identify

potential signatures of physics beyond general relativity and the Standard Model.

Acknowledgments. The authors acknowledge the support from the Simons Foundation through Award No. 896696, the NSF through Grant No. PHY-2207650 and NASA through Grant No. 80NSSC22K0806. The authors thank Emanuele Berti, Mark Cheung, Carl-Johan Haster, Kelvin K.H. Lam, Hector O Silva, Isaac C.F. Wong, and Sophia Yi for insightful discussion. A. K. W. C would like to thank Simon Maenaut and Gregorio Carullo for advise on preparing and sharing the configuration files for `pyRing` analyses. The calculations and results reported in this Letter were produced using the computational resources of the Illinois Campus Cluster, a computing resource that is operated by the Illinois Campus Cluster Program (ICCP) in conjunction with National Center for Supercomputing Applications (NCSA), and is supported by funds from the University of Illinois at Urbana-Champaign, and used Delta at NCSA through allocation PHY240142 from the Advanced Cyberinfrastructure Coordination Ecosystem: Services & Support (ACCESS) program, which is supported by National Science Foundation Grants No. 2138259, No. 2138286, No. 2138307, No. 2137603, and No. 2138296. The author would like to specially thank the investors of the IlliniComputes initiatives and GravityTheory computational nodes for permitting the authors to execute runs related to this work using the relevant computational resources.

Appendix A: Quasinormal-mode spectra in axi-dilaton gravity

In this section, we provide a heuristic argument to show that the leading-order-in- ζ frequency shift of the quasinormal-mode frequencies in axi-dilaton gravity is the sum of that in dynamical Chern-Simons and scalar Gauss-Bonnet gravity.

Applying the least action principle to the Lagrangian, we obtain the following equations of motion,

$$R_{\mu}^{\nu} + \zeta [(\mathcal{M}_{\mu}^{\nu})_{\text{dCS}} + (\mathcal{M}_{\mu}^{\nu})_{\text{sGB}}] = 0, \quad (\text{A1})$$

$$\square \vartheta_1 + \mathcal{G} = 0, \quad \text{and} \quad \square \vartheta_2 + \mathcal{P} = 0, \quad (\text{A2})$$

where we have written $\varphi_{1,2} = \alpha \vartheta_{1,2}$, defined $\zeta := \alpha^2/M^4$ as a dimensionless coupling parameter, with M the source-frame black-hole mass, $\alpha_1 = \alpha_2 := \ell_{\text{AD}}^2 = \alpha$ is the coupling constant, and $\square = (-g)^{-\frac{1}{2}} \partial_{\gamma} \left((-g)^{\frac{1}{2}} g^{\gamma\lambda} \partial_{\lambda} \right)$ is the d'Alembertian operator. The quantities $(\mathcal{M}_{\mu}^{\nu})_{\text{dCS}}$ and $(\mathcal{M}_{\mu}^{\nu})_{\text{sGB}}$ are rank-2 tensors that are defined through the curvature tensor and the derivative of $\vartheta_{1,2}$, namely [24, 28]

$$\begin{aligned} (\mathcal{M}_{\mu}^{\nu})_{\text{dCS}} &= -4g_{\mu\beta} \nabla_{\rho} \nabla_{\sigma} \left[\tilde{R}^{\rho(\beta\nu)\sigma} \vartheta_2 \right] - \frac{1}{2} \nabla_{\mu} \vartheta_2 \nabla^{\nu} \vartheta_2, \\ (\mathcal{M}_{\mu}^{\nu})_{\text{sGB}} &= \delta_{\mu\lambda\gamma\delta}^{\nu\sigma\alpha\beta} R^{\gamma\delta}{}_{\alpha\beta} \nabla^{\lambda} \nabla_{\sigma} \vartheta_1 \\ &\quad - \frac{1}{2} \delta_{\mu}^{\nu} \delta_{\eta\lambda\gamma\delta}^{\eta\sigma\alpha\beta} R^{\gamma\delta}{}_{\alpha\beta} \nabla^{\lambda} \nabla_{\sigma} \vartheta_1, \\ &\quad - \frac{1}{2} \nabla_{\mu} \vartheta_1 \nabla^{\nu} \vartheta_1. \end{aligned} \quad (\text{A3})$$

Given the equations of motion, we can in principle solve for the scalar field, $\vartheta_{1,2}$, via

$$\begin{aligned} \vartheta_1 &= -\square^{-1} \mathcal{G}, \\ \vartheta_2 &= -\square^{-1} \mathcal{P}, \end{aligned} \quad (\text{A4})$$

where \square^{-1} is the inverse of the d'Alembertian operator. Substituting these expressions back into the tensor equations, we can formulate the equations of motion without explicitly involving the scalar fields. More specifically, we can rewrite the tensor corrections as

$$\begin{aligned} (\mathcal{M}_{\mu}^{\nu})_{\text{dCS}} &= 4g_{\mu\beta} \nabla_{\rho} \nabla_{\sigma} \left[\tilde{R}^{\rho(\beta\nu)\sigma} \square^{-1} \mathcal{P} \right] \\ &\quad - \frac{1}{2} \nabla_{\mu} (\square^{-1} \mathcal{P}) \nabla^{\nu} (\square^{-1} \mathcal{P}), \\ (\mathcal{M}_{\mu}^{\nu})_{\text{sGB}} &= -\delta_{\mu\lambda\gamma\delta}^{\nu\sigma\alpha\beta} R^{\gamma\delta}{}_{\alpha\beta} \nabla^{\lambda} \nabla_{\sigma} (\square^{-1} \mathcal{G}) \\ &\quad + \frac{1}{2} \delta_{\mu}^{\nu} \delta_{\eta\lambda\gamma\delta}^{\eta\sigma\alpha\beta} R^{\gamma\delta}{}_{\alpha\beta} \nabla^{\lambda} \nabla_{\sigma} (\square^{-1} \mathcal{G}), \\ &\quad - \frac{1}{2} \nabla_{\mu} (\square^{-1} \mathcal{G}) \nabla^{\nu} (\square^{-1} \mathcal{G}). \end{aligned} \quad (\text{A5})$$

By solving the tensor field equations, we can construct the background space-time of a stationary black hole in

axi-dilaton gravity. To first order in ζ , we can decompose the metric tensor as

$$g_{\mu\nu} = g_{\mu\nu}^{(0)} + \zeta g_{\mu\nu}^{(1)}, \quad (\text{A6})$$

where $g_{\mu\nu}^{(0)}$ stands for the Kerr metric in general relativity and $g_{\mu\nu}^{(1)}$ is the axi-dilaton deformation. In [24], $g_{\mu\nu}^{(1)}$ is solved for as a power series in a , r^{-1} and χ . For axi-dilaton gravity, $g_{\mu\nu}^{(1)}$ is just the sum of that in dynamical Chern-Simons and scalar Gauss-Bonnet gravity simply because non-linear interactions between the scalars ϑ_1 and ϑ_2 lead to quadratic (and higher-order) terms in ζ .

Let us now consider quasinormal-mode metric perturbations in the Boyer-Lindquist coordinates $x^{\mu} = (t, r, \chi = \cos \iota, \phi)$. In these coordinates, the perturbed metric can be written as

$$g_{\mu\nu} = g_{\mu\nu}^{\text{GR}} + \zeta g_{\mu\nu}^{(1)} + \varepsilon e^{im\phi - i\omega t} \hat{h}_{\mu\nu}(r, \chi), \quad (\text{A7})$$

where $\varepsilon \ll 1$ is a bookkeeping parameter for the perturbations, m and ω are the magnetic mode number and the complex frequency of the perturbations. Let us denote the perturbations of N_{ζ} -th order in ζ and N_{ε} -th order in ε to a rank-2 tensor with a superscript $(N_{\zeta}, N_{\varepsilon})$. In this notation, we see that

$$[R_{\mu}^{\nu}]^{(1,1)} + \zeta [(\mathcal{M}_{\mu}^{\nu})_{\text{dCS}}]^{(0,1)} + \zeta [(\mathcal{M}_{\mu}^{\nu})_{\text{sGB}}]^{(0,1)} = 0, \quad (\text{A8})$$

which immediately implies that metric perturbations at first-order in ζ is the sum of two parts, each of which is sourced by the linearization of the dynamical Chern-Simons terms $[(\mathcal{M}_{\mu}^{\nu})_{\text{dCS}}]^{(0,1)}$ and the scalar Gauss-Bonnet terms $[(\mathcal{M}_{\mu}^{\nu})_{\text{sGB}}]^{(0,1)}$ on the Kerr background. From this equation, it already follows that the leading-order-in- ζ frequency shift of the quasinormal-mode frequencies in axi-dilaton gravity is the sum of that in the two gravity theories.

To be more specific, let us solve Eq. (A8) using METRICS. To simplify the problem, we enforce the Regge-Wheeler gauge, which many quadratic-gravity theories have sufficient gauge degrees of freedom to enforce [46]. In this gauge, the metric perturbations are completely specified by 6 unknowns, which we write $h_{j=1,2,\dots,6}$. Since $\hat{h}_{\mu\nu}$ is purely ingoing at the horizon and purely outgoing at spatial infinity, h_j is diverging at these two boundaries. Before we perform spectral expansions on h_j , we need to construct an asymptotic factor $A_j(r)$ to accommodate this divergent behaviour. An explicit form of $A_j(r)$ can be specified via the surface gravity and angular velocity of the event horizon of the black hole. Using the $A_j(r)$ asymptotic factor, the h_j functions admit a spectral expansion that can be written schematically as

$$h_j = A_j(r) \sum_{p=1}^N \sum_{\ell=1}^N v_{j,p,\ell} \varphi_{p,\ell}(r, \chi), \quad (\text{A9})$$

where no sum on j is implied, $\varphi_{p,\ell}(r, \chi)$ is a complete and orthogonal spectral basis of r and χ , and the $v_{j,p,\ell}$ are constants.

Substituting Eq. A9 into Eq. A7, and then substituting the result into Eq. A1, we expand the tensor field equations to first order in ε and obtain a system of homogeneous linear algebraic equations for the coefficients $v_{j,p,\ell}$. Let us define the vector \mathbf{v} to collect all components of $v_{j,p,\ell}$, namely $\mathbf{v} = \{v_{j,p,\ell}\}$. With this notation, the algebraic system can be written as

$$\mathbb{D}(\omega) \cdot \mathbf{v} = \left[\mathbb{D}^{(0)}(\omega) + \zeta \mathbb{D}^{(1)}(\omega) \right] \cdot \mathbf{v} = \mathbf{0}, \quad (\text{A10})$$

where $\mathbb{D}(\omega)$ is a rectangular matrix of dimension $10N^2 \times 6N^2$, whose entries depend on the frequency ω and background parameters M_z , a , and M_z . Since Eq. (A10) is valid only to first order in ζ , we seek solutions that are also accurate to this order. To proceed, we specify one component of $\mathbf{v}^{(0)}$ and $\mathbf{v}^{(1)}$, as in Refs. [13, 15]. The remaining undetermined components of $\mathbf{v}^{(0)}$ ($\mathbf{v}^{(1)}$), together with $\omega^{(0)}$ ($\omega^{(1)}$), are collected into vectors $\mathbf{x}^{(0)}$ ($\mathbf{x}^{(1)}$) respectively. Applying the spectral perturbation theory developed in METRICS, we obtain

$$\mathbf{x}^{(1)} = -\mathbb{J}^{-1} \cdot \left(\mathbb{D}^{(1)} \Big|_{\omega^{(0)}} \cdot \mathbf{v}^{(0)} \right), \quad (\text{A11})$$

where $\mathbb{J} = \partial_{\mathbf{x}^{(0)}} \mathbb{D}^{(0)}$ is the Jacobian matrix, and \mathbb{J}^{-1} denotes its generalized inverse. The first-order-in- ζ terms in Eq. (A1) consist of a group terms that follow from dynamical Chern-Simons gravity and another group from scalar Gauss-Bonnet gravity. Naturally, we can then write

$$\mathbb{D}^{(1)}(\omega) = \mathbb{D}_{\text{dCS}}^{(1)}(\omega) + \mathbb{D}_{\text{sGB}}^{(1)}(\omega), \quad (\text{A12})$$

where $\mathbb{D}_{\text{dCS}}^{(1)}(\omega)$ is the coefficient matrix obtained from performing an spectral expansion on $(\mathcal{M}_\mu^\nu)_{\text{dCS}}$, and $\mathbb{D}_{\text{sGB}}^{(1)}(\omega)$ is the coefficient matrix from $(\mathcal{M}_\mu^\nu)_{\text{sGB}}$. Then, it follows from Eq. (A11) that

$$\omega_{\text{AD}}^{(1)} = \omega_{\text{dCS}}^{(1)} + \omega_{\text{sGB}}^{(1)}. \quad (\text{A13})$$

Similar arguments can also be constructed using the modified Teukolsky formalism.

Appendix B: Further robustness checks of the results

In this section of Supplemental Material, we perform multiple checks of robustness and of the correctness of our results. As observed from Fig. 1, the marginalized ℓ posterior of different quadratic-gravity theories inferred from different signals is similar. Thus, except for the assessment of parameter degeneracies, we will focus on tests of dynamical Chern-Simons gravity using the ringdown signal of GW150914 as an example; we expect qualitatively similar conclusions to hold when analyzing different ringdown signals.

1. Consistency with the small-coupling approximation

The left panel of Fig. 2 shows the marginalized posterior of ζ as a function of ℓ for axi-dilaton (solid), dynamical Chern-Simons (dashed), and scalar Gauss-Bonnet (dotted) gravity, derived from samples of M_z , d_L , and ℓ using Eq. (4), based on the GW150914 ringdown signal. In the interest of space, we only show the posteriors of $\zeta < 0.2$, as the posteriors beyond this range have negligible support. Observe that most of the samples lie within the $\zeta \lesssim 0.2$ region. Note also that $\zeta \lesssim \mathcal{O}(10^{-1})$ denotes the regime of coupling parameter space that is consistent with the small-coupling approximation. This justifies the use of the METRICS quasinormal-mode frequencies, which are only valid up to first order in ζ . Furthermore, the posterior of ζ shows that the posterior of ℓ is not an artifact of excluding values of ℓ that lead to $\zeta > 1$.

We also verified that the posterior is not affected by the exclusion of values of ℓ in the prior that lead to $\text{Im}(\omega) > 0$ (see discussion in the last paragraph of the parameter estimation section). The right panel of Fig. 2 shows the marginalized posterior of ℓ of dynamical Chern-Simons gravity inferred from the GW150914 ringdown signal using two priors: one excluding $\text{Im}(\omega) > 0$ (solid blue) and another excluding $\text{Im}(\omega) > -0.1$ (dashed blue). Observe that the two posteriors overlap almost completely, indicating that adjusting the exclusion region of $\text{Im}(\omega)$ within a reasonable range does not significantly affect our constraints on quadratic-gravity theories. The 90% confidence levels on ℓ obtained by excluding $\text{Im}(\omega) > 0$ and $\text{Im}(\omega) > -0.1$ are 53.6 km and 53.7 km, respectively. In other words, our posteriors are not sensitive to the precise cut-off chosen for $\text{Im}(\omega)$.

2. Degeneracy amongst ℓ , M and a

Figure 3 shows the 90% confidence intervals of the two-dimensional marginalized posteriors in the M_z - a (left), M_z - ℓ (middle), and a - ℓ (right) planes, obtained from the analysis of the ringdown phase of GW150914 assuming different gravity theories: general relativity (GR; solid black, shown only in the left panel), axi-dilaton (solid blue), dynamical Chern-Simons (dashed red), and scalar Gauss-Bonnet (dash-dotted green) gravity. In the left panel, observe that the general relativity posterior is consistent with previous studies [41, 47] and it lies close to the LIGO-Virgo-KAGRA median values ([48], marked by \times), confirming the validity of our general relativity inference. The posteriors obtained using quadratic gravity models are not significantly distorted, suggesting no strong degeneracy between ℓ , M_z , and a . This conclusion is supported by the middle and right panels. The vertical solid black lines indicate the LIGO-Virgo-KAGRA median remnant mass (middle panel) and spin (right panel). All confidence intervals show no significant degeneracies in the M_z - ℓ or a - ℓ planes, confirming that ℓ is not strongly correlated

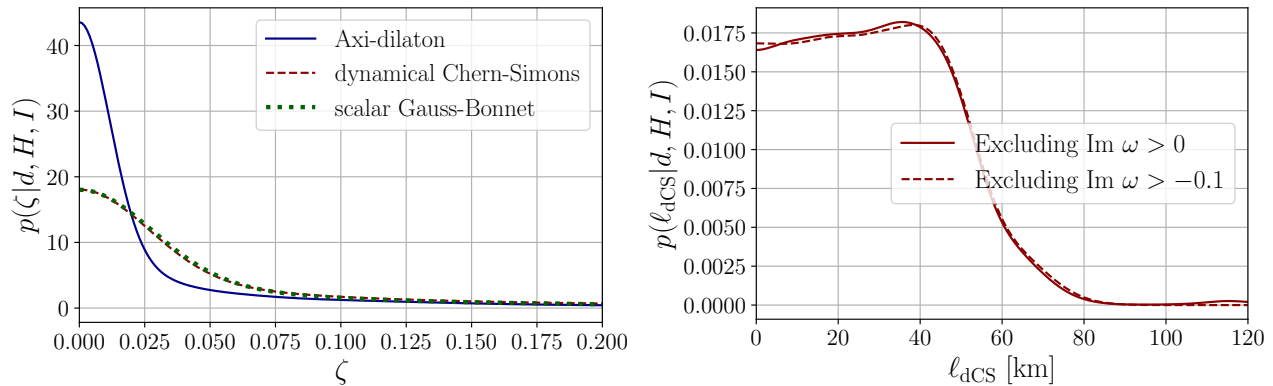


FIG. 2. (Left panel) Marginalized posterior distribution of ζ , obtained by converting the samples of d_L , M_z and ℓ inferred from the GW150914 ringdown signal via Eq. 4. We only show the posterior up to $\zeta = 0.2$, as the posterior has only negligible support for $\zeta > 0.2$. Observe that most of the ζ samples are within 0.2, indicating the close consistency between the results of our analyses with the small-coupling approximation. (Right panel) Marginalized posterior distribution of ℓ , inferred from the GW150914 ringdown signal, using priors that exclude $\text{Im}(\omega) > 0$ (solid blue) and $\text{Im}(\omega) > -0.1$ (dashed blue). Observe that the two posteriors are nearly identical, indicating that the results are not sensitive to the exact $\text{Im}(\omega)$ cut-off. We conclude that the posterior of ℓ is not driven by the exclusion of $\zeta > 1$ or $\text{Im}(\omega) > 0$ from the prior.

with the remnant properties. We thus conclude that our constraints on ℓ are robust and do not compromise the accuracy of the inferred remnant mass and spin.

3. Convergence of Bayesian inference

Fig. 4 shows the posterior of ℓ in dynamical Chern-Simons gravity inferred from the GW150914 ringdown, using nested sampling with 4096 live points for two random seeds (solid and dashed) and 2048 live points (dotted). The 90-% confidence intervals on ℓ of these three posteriors are 53.6 km, 53.5 km, and 52.9 km, respectively. The close agreement among all posteriors indicates the convergence of our Bayesian inference.

4. The approximation of $A_{nlm}^{N,q} = (-1)^l (A_{nlm}^{P,q})^\dagger$

The assumption $A_{nlm}^{N,q} = (-1)^l (A_{nlm}^{P,q})^\dagger$ is not required, but it reduces the number of free parameters and accelerates sampling. Figure 5 shows the posterior of ℓ in dynamical Chern-Simons gravity inferred from the GW150914 ringdown, with (solid) and without (dashed) imposing this relation. The 90-% confidence intervals on ℓ obtained by assuming and not assuming $A_{nlm}^{N,q} = (-1)^l (A_{nlm}^{P,q})^\dagger$ are 53.7 km and 55.9 km, respectively. The two posteriors are nearly identical, indicating that the assumption has negligible impact on the constrain on ℓ .

5. Robustness against the uncertainty in the METRICS frequencies

The numerical errors in the METRICS computations lead to uncertainty in the fitted coefficients of the METRICS quasinormal-mode frequencies. The proper way to account for this uncertainty is to treat the coefficients as free parameters with a multivariate Gaussian prior, using the known variance-covariance matrix of the fitting coefficients. However, this approach significantly increases the number of inference parameters and the computational cost of nested sampling. To estimate the impact of numerical error of the METRICS frequencies, we construct a polynomial fit to the best-fit 022-mode frequencies shifted by $\pm 1\sigma$, as shown in Fig. 6. Observe that at large spin, where the numerical error is the largest, the error is, at most, as large as the size of the scattered symbols. After taking the numerical error in METRICS frequencies at all spins into account, the values of the frequencies computed using different fitting functions are not changed much at all.

Figure 7 presents the inferred posterior of ℓ in dynamical Chern-Simons gravity, using the fitting polynomial to the best-fit frequencies shifted by $+1\sigma$ (dashed) and -1σ (dotted), which is to be compared with the posterior obtained using fitting expressions to the best-fit frequencies (solid). As shown in this figure, the posteriors are consistent with each other because, given the sensitivity of the existing detectors, the statistical error of the detection dominates the systematic errors induced by the numerical errors in the METRICS frequencies. The 90-% confidence intervals on ℓ obtained using the best-fit frequency, shifted by $+1\sigma$ and -1σ is 53.6 km, 55.2 km and 54.7 km respectively. Thus, we conclude that, even if we infer the fitting coefficients as free parameters, the 90-%

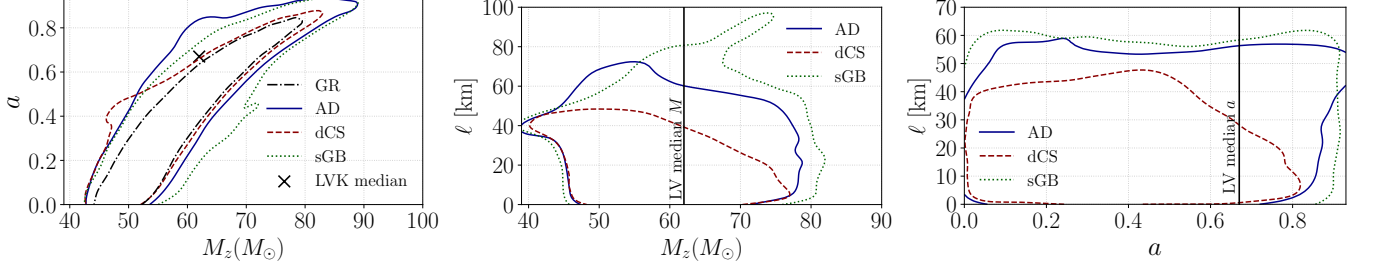


FIG. 3. The 90% confidence interval of the marginalized two-dimensional posteriors in the M_z - a (left), M_z - ℓ (middle), and a - ℓ (right) planes, inferred from the ringdown phase of GW150914 assuming axi-dilaton (solid blue), dynamical Chern–Simons (dashed red), scalar Gauss–Bonnet (dotted green) gravity theories, and general relativity (dashed-dotted black, shown only in the left panel). Observe that the general-relativity contour lies very close to the median remnant mass and spin reported by the LIGO–Virgo–KAGRA collaboration (marked by \times , labeled “LVK median”), validating our general-relativity ringdown analysis. Observe also that the inclusion of ℓ does not induce significant distortion to the contours, implying that there should be no strong correlations between ℓ and either M_z or a . The deduction is further consolidated by the observation that the contours in the M_z – ℓ and a – ℓ planes exhibit no significant inclination.

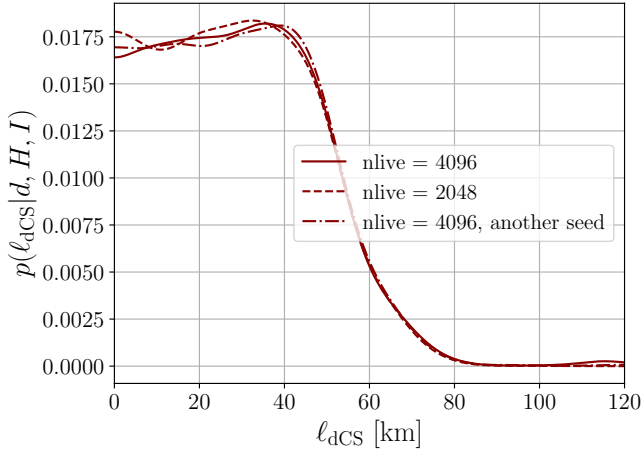


FIG. 4. The marginalized posterior distribution of the coupling parameter ℓ in dynamical Chern–Simons gravity is shown, as sampled from the ringdown signal of GW150914. The results are obtained using nested sampling with 4096 live points for two different random seeds (solid and dotted lines) and with 2048 live points (dashed line). All three posteriors are in good agreement with each other, demonstrating the robustness and convergence of the nested sampling procedure.

confidence interval will not be affected much at all. In other words, our results are robust against the numerical uncertainties in the METRICS frequencies.

6. Robustness against the systematic errors in the quasinormal-mode spectra model for spins $a > 0.75$

As discussed, nested sampling occasionally explores regions with $a > 0.75$, where the quasinormal-mode spectra in dynamical Chern–Simons (and hence axi-dilaton) gravity, computed using METRICS, have not been calculated

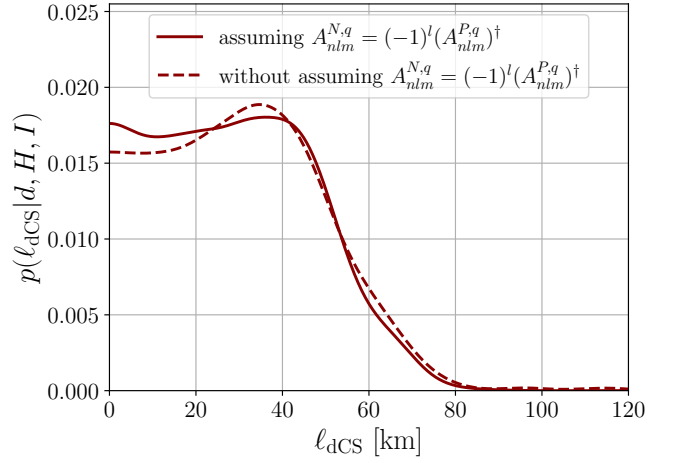


FIG. 5. The marginalized posterior of ℓ_{dCS} obtained by analyzing GW150914 ringdown signal, assuming (solid blue) and without approximating (dashed blue) $A_{nlm}^{N,q} = (-1)^l (A_{nlm}^{P,q})^\dagger$. Observe that the two posteriors overlay almost on top of each other, indicating that the constraint on ℓ is not significantly impacted by the approximation.

accurately yet. To assess the impact of this limitation, we manufacture two mock-ups of possible 022-mode spectra as follows. First, we extrapolate the axial and polar 022-mode frequencies up to $a = 0.93$ using the existing fitting expressions. Then, we artificially displace both the real and imaginary parts of the frequencies at $a = 0.93$ by ± 0.4 and ± 0.1 , respectively. These displacements are chosen because we found that these are approximately the error of the corresponding parts of the Kerr 022-mode frequency at $a = 0.93$, if one extrapolates the frequency from $a = 0.753$ using the same number of frequencies and fitting polynomial of the same degree. We refer to these models as “mock spectra 1” and “mock spectra 2”. We fit each mock spectrum using a polynomial of one

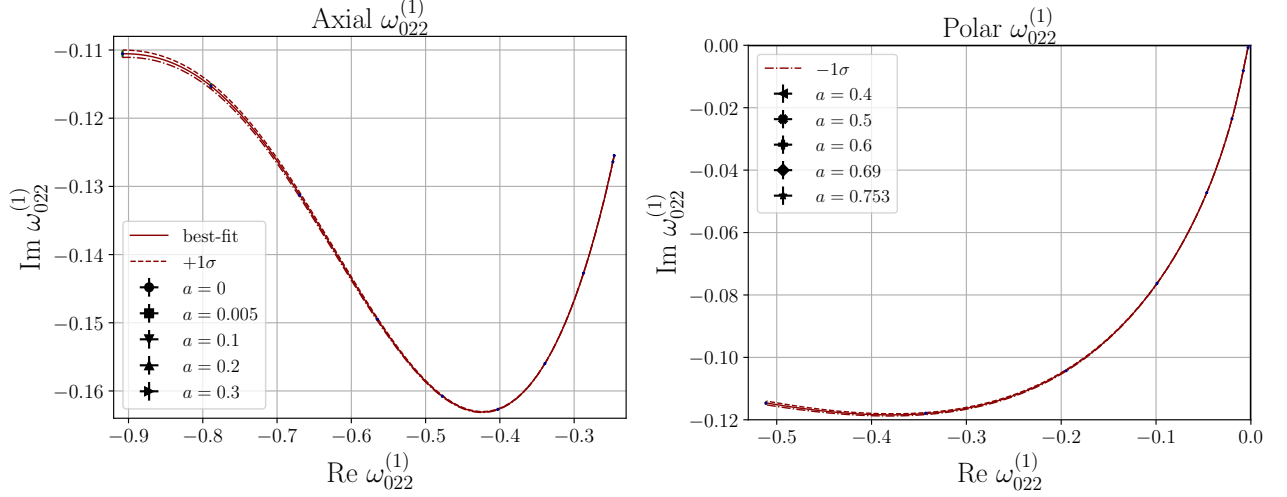


FIG. 6. Trajectories in the complex plane traced by the METRICS 022-mode axial (left) and polar (right) frequencies in dynamical Chern-Simons gravity. The different symbols correspond to the numerical frequencies calculated with METRICS with numerical error bars (small vertical lines in green, which are usually not visible because they are smaller than the symbol size) at different spin values. The solid, dashed and dot-dash curves correspond to the a polynomial fit to the frequencies, a fit to the frequencies shifted by $+1\sigma$, and a fit to the frequencies shifted by -1σ , respectively, where σ is the 1σ -numerical error of the frequencies at different spin values (c.f. Table. II of [17]). Observe that the numerical error at small spin is much smaller than that at a large spin, and that the dashed and dot-dashed curves are very close to the solid curve.

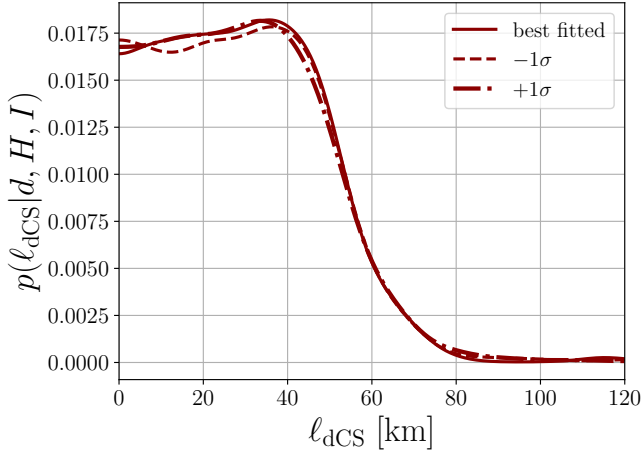


FIG. 7. The marginalized posterior of ℓ in dynamical Chern-Simons gravity inferred from the GW150914 ringdown phase, using the METRICS 022-mode frequency at their best-fit values (solid), and shifted by $+1\sigma$ (dashed) and -1σ (dotted). The close agreement among the posteriors demonstrates the robustness of our results against numerical uncertainties in the METRICS frequencies and their fitted coefficients.

degree higher than the optimal degree used in the original fits. We check that the frequencies computed using the fitting expressions of these spectra are different from the mock data by only $\sim 10^{-3}$ for $a \leq 0.75$. Figure 8 shows the axial (left) and polar (right) 022-mode frequencies in the complex plane, comparing the original fits (solid lines), the METRICS frequencies (scatters, taken from

[17]), and the two mock spectra (dashed and dash-dotted lines). All spectra agree well for $a \leq 0.753$, beyond which they diverge from each other, forming a broad spread in the complex plane that reflects the uncertainty in the quasinormal-mode spectrum at very large spins.

Figure 9 shows the marginalized posterior of ℓ in dynamical Chern-Simons gravity obtained using the original spectra (solid) and the two mock spectra models (dashed and dotted). Observe that the posteriors are largely consistent with each other. The 90-% confidence interval on ℓ obtained using the METRICS spectra is 53.6 km, while using the first and second mock spectra the 90% confidence interval is 54.2 km and 53.4 km, respectively. The latter two 90% confidence intervals are not significantly affected regardless of the dependence of the quasinormal-mode spectra on $a > 0.753$, demonstrating the robustness of our results against the ignorance of the dependence of quasinormal-mode frequencies at $a > 0.75$. This robustness is expected, given that, as shown in Fig. 3, most of the posterior support lies inside $a < 0.75$.

7. Robustness against uncertainty in the ringdown start time

We also checked that our results are robust against the choice of the ringdown start time. Figure 10 shows the posterior of ℓ in dynamical Chern-Simons gravity inferred from the GW150914 ringdown signal, assuming the ringdown signal starts at $9M_z$ (dashed-dotted), $10M_z$ (solid) and $11M_z$ (dotted) after the time when the amplitude

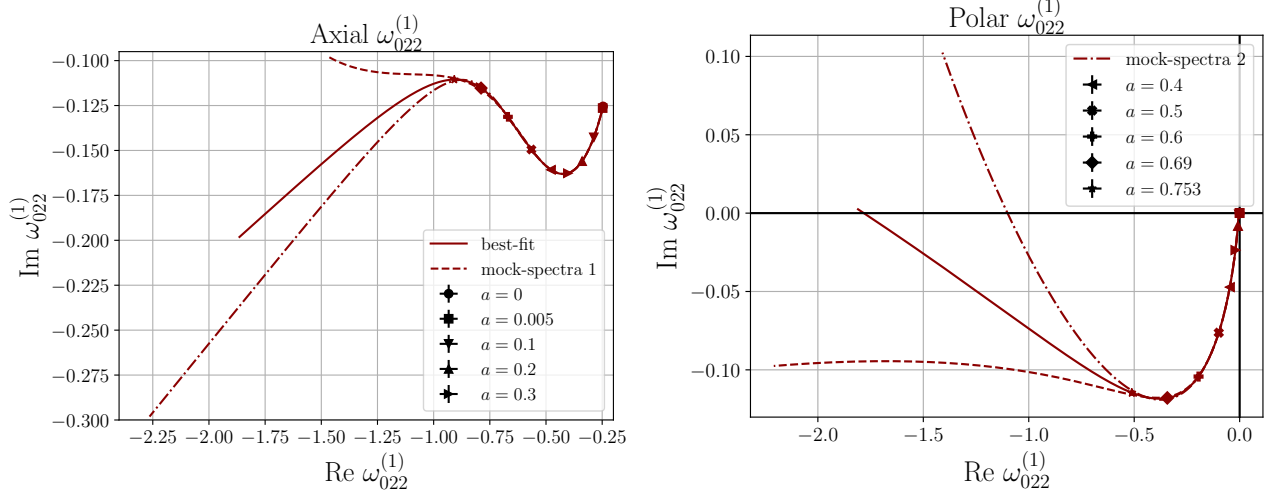


FIG. 8. Quasinormal-mode frequencies of the axial (left) and polar (right) 022 modes, computed using the original fitting expressions to the METRICS data (solid lines) and two mock spectra (dashed and dash-dotted lines). The scatters mark frequencies computed from METRICS [17]. For $a \leq 0.753$, all spectra show good agreement. Beyond this spin, the mock spectra diverge, spanning a broad region in the complex plane that represents the estimated uncertainty in the quasinormal-mode frequencies at high spin.

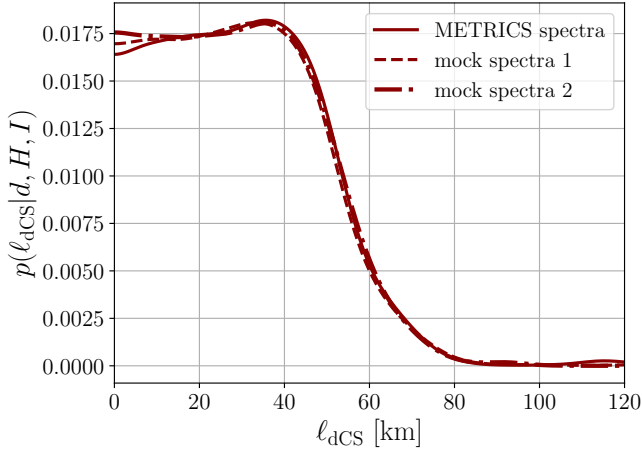


FIG. 9. Marginalized posterior distribution of ℓ in dynamical Chern–Simons gravity inferred from the GW150914 ringdown signal, using the fitting expression for the METRICS frequencies (solid) and using the two mock spectra models (dashed and dash-dotted; see Fig. 8 and main text of the Supp. Mat.). The posteriors almost overlay on top of each other, indicating that our results are robust against the ignorance of the quasinormal-mode spectra for spins $a > 0.753$.

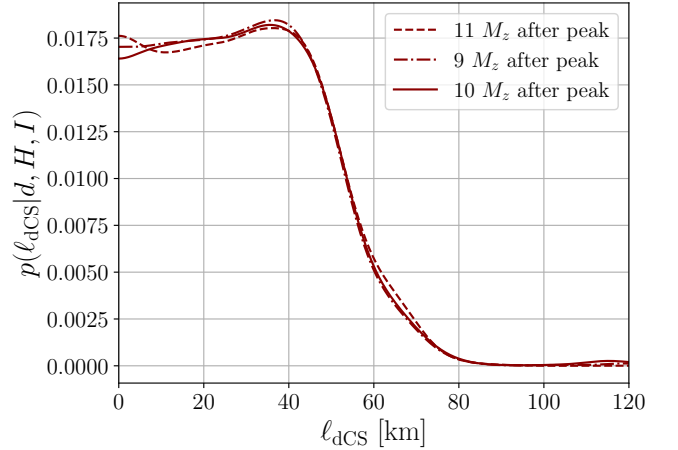


FIG. 10. Marginalized posterior distribution of ℓ in dynamical Chern–Simons gravity inferred from the GW150914 ringdown signal, assuming the ringdown phase starts at $9M_z$ (dash-dotted), $10M_z$ (solid), and $11M_z$ (dashed) after the peak of $h_+^2 + h_\times^2$. Here, M_z is the remnant mass estimated from a full waveform analysis in general relativity. The near-identical posteriors indicate that the results are robust against the choice of ringdown start time.

$h_+^2 + h_\times^2$ is peaked. The 90-% confidence intervals on ℓ obtained assuming the ringdown phase starts at $9M_z$, $10M_z$, and $11M_z$ are 52.9 km, 53.6 km, and 53.7 km, respectively. All posteriors are consistent with each other, indicating that our results are robust against difference choices of the ringdown start time, provided that the non-linearity has been well subsided and a reasonable signal-to-noise

ratio is able to be recovered by the choices.

8. Effects of the inclusion of an overtone

To assess the impact of including an overtone, we infer the posterior of ℓ using both the $nlm = 022$ and 122 modes.

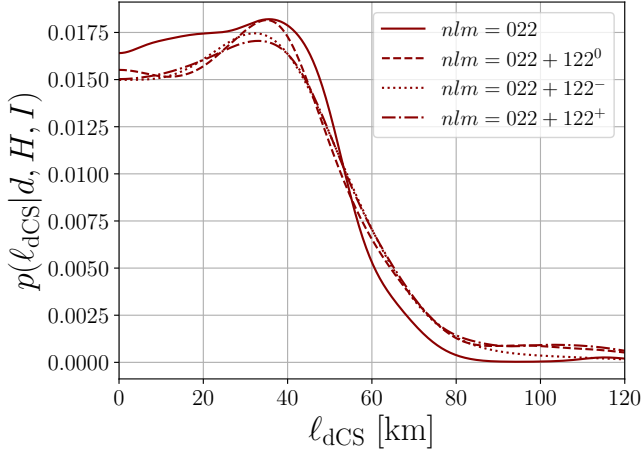


FIG. 11. Marginalized posterior distribution of ℓ in dynamical Chern–Simons gravity inferred from the GW150914 ringdown phase, using the waveform model in Eq. 2 with different mode combinations: the $nlm = 022$ mode alone (solid), the $022 + 122^{(0)}$ modes (dashed), the $022 + 122^-$ modes (dotted), and the $022 + 122^+$ modes (dash-dotted). The $122^{(0)}$ frequencies are estimated using the modified Teukolsky formalism, valid to first order in spin. The 122^- (122^+) modes are synthetic spectra constructed by decreasing (increasing) the real and imaginary parts of the $122^{(0)}$ frequencies at $a = 0.75$ by 100%, linearly interpolated with the unmodified $a = 0$ value. The close agreement among all posteriors demonstrates that including an overtone does not substantially affect the inferred constraint on ℓ , even with significant uncertainty in the overtone frequencies.

The overtone frequencies of black holes with $a \geq 0.75$ in dynamical Chern–Simons gravity have yet to be accurately computed. The most up-to-date estimates come from the modified Teukolsky formalism, which is valid only to first order in spin. In our analysis here, we adopt the 122-mode

frequencies computed using this formalism, denoted as the $nlm = 122^0$ spectrum, along with the METRICS 022-mode frequencies, to infer the posterior of ℓ . However, by comparing the METRICS frequencies (accurate to $a \sim 0.8$) with their first-order-in-spin counterparts, we find relative differences of up to 100% [13, 17]. To account for this uncertainty, we construct two additional sets of synthetic 122-mode spectra. Specifically, we first evaluate the 122^0 frequencies at $a = 0.75$, and then we artificially increase or decrease both their real and imaginary parts by 100%, while keeping the values at $a = 0$ unchanged. We then perform a linear fit between the $a = 0$ values and the modified $a = 0.75$ points to create two new spectra: one with amplified values (122^+) and one with suppressed values (122^-).

Figure 11 shows the marginalized posterior of ℓ in dynamical Chern–Simons gravity inferred using different mode combinations: the 022 mode alone (solid line), $022 + 122^0$ (dashed), $022 + 122^-$ (dotted), and $022 + 122^+$ (dash-dotted). All posteriors are largely consistent with one another. The 90% confidence interval on ℓ is 53.6 km using only the 022 mode, and 62.1 km, 62.3 km, and 62.9 km when including the 122^0 , 122^- , and 122^+ modes, respectively. Clearly, the constraints weaken when introducing higher modes in the fitting, because these additional modes do not contribute enough information to the likelihood², while they do enlarge the prior volume. In fact, the signal evidence obtained using the waveform model that contains both the $nlm = 022$ and 122^0 modes is about $\exp(2.29) \approx 10$ times smaller than that using just the 022 mode. Nonetheless, the 90% confidence limits are still very similar to each other, and the overall shape of the posteriors is also similar. These results demonstrate that the inclusion of an overtone does not have a significant impact on the inferred constraints, and, in particular, they do not significantly alter the posterior.

-
- [1] N. Yunes, X. Siemens, and K. Yagi, “Gravitational-Wave Tests of General Relativity with Ground-Based Detectors and Pulsar-Timing Arrays,” (2024), [arXiv:2408.05240 \[gr-qc\]](#).
 - [2] X. Calmet, M. Graesser, and S. D. H. Hsu, “Minimum length from quantum mechanics and general relativity,” *Phys. Rev. Lett.* **93**, 211101 (2004), [arXiv:hep-th/0405033](#).
 - [3] S. Perlmutter *et al.* (Supernova Cosmology Project), “Measurements of Ω and Λ from 42 high redshift supernovae,” *Astrophys. J.* **517**, 565–586 (1999), [arXiv:astro-ph/9812133](#).
 - [4] A. G. Riess *et al.* (Supernova Search Team), “Observational evidence from supernovae for an accelerating

universe and a cosmological constant,” *Astron. J.* **116**, 1009–1038 (1998), [arXiv:astro-ph/9805201](#).

- [5] Y. Sofue and V. Rubin, “Rotation curves of spiral galaxies,” *Ann. Rev. Astron. Astrophys.* **39**, 137–174 (2001), [arXiv:astro-ph/0010594](#).
- [6] G. Bertone and D. Hooper, “History of dark matter,” *Rev. Mod. Phys.* **90**, 045002 (2018), [arXiv:1605.04909 \[astro-ph.CO\]](#).
- [7] B. P. Abbott *et al.* (LIGO Scientific, Virgo), “GWTC-1: A Gravitational-Wave Transient Catalog of Compact Binary Mergers Observed by LIGO and Virgo during the First and Second Observing Runs,” *Phys. Rev. X* **9**, 031040 (2019), [arXiv:1811.12907 \[astro-ph.HE\]](#).
- [8] R. Abbott *et al.* (LIGO Scientific, Virgo), “GWTC-2: Compact Binary Coalescences Observed by LIGO and Virgo During the First Half of the Third Observing Run,” *Phys. Rev. X* **11**, 021053 (2021), [arXiv:2010.14527 \[gr-qc\]](#).
- [9] R. Abbott *et al.* (LIGO Scientific, VIRGO, KAGRA), “GWTC-3: Compact Binary Coalescences Observed by LIGO and Virgo During the Second Part of the Third

² This is because we are starting the quasi-normal fitting in the quasi-linear regime, about $10M_z$ after the peak of the amplitude, where higher overtones are subdominant to the dominant mode and do not contribute much signal-to-noise ratio.

- Observing Run,” (2021), [arXiv:2111.03606 \[gr-qc\]](#).
- [10] B. P. Abbott *et al.* (LIGO Scientific, Virgo), “Tests of General Relativity with the Binary Black Hole Signals from the LIGO-Virgo Catalog GWTC-1,” *Phys. Rev. D* **100**, 104036 (2019), [arXiv:1903.04467 \[gr-qc\]](#).
 - [11] R. Abbott *et al.* (LIGO Scientific, Virgo), “Tests of general relativity with binary black holes from the second LIGO-Virgo gravitational-wave transient catalog,” *Phys. Rev. D* **103**, 122002 (2021), [arXiv:2010.14529 \[gr-qc\]](#).
 - [12] R. Abbott *et al.* (LIGO Scientific, VIRGO, KAGRA), “Tests of General Relativity with GWTC-3,” (2021), [arXiv:2112.06861 \[gr-qc\]](#).
 - [13] A. K.-W. Chung and N. Yunes, “Quasinormal mode frequencies and gravitational perturbations of black holes with any subextremal spin in modified gravity through METRICS: The scalar-Gauss-Bonnet gravity case,” *Phys. Rev. D* **110**, 064019 (2024), [arXiv:2406.11986 \[gr-qc\]](#).
 - [14] E. Berti *et al.*, “Black hole spectroscopy: from theory to experiment,” (2025), [arXiv:2505.23895 \[gr-qc\]](#).
 - [15] A. K.-W. Chung, P. Wagle, and N. Yunes, “Spectral method for metric perturbations of black holes: Kerr background case in general relativity,” *Phys. Rev. D* **109**, 044072 (2024), [arXiv:2312.08435 \[gr-qc\]](#).
 - [16] A. K.-W. Chung and N. Yunes, “Ringing out General Relativity: Quasinormal Mode Frequencies for Black Holes of Any Spin in Modified Gravity,” *Phys. Rev. Lett.* **133**, 181401 (2024), [arXiv:2405.12280 \[gr-qc\]](#).
 - [17] A. K.-W. Chung, K. K.-H. Lam, and N. Yunes, “Quasinormal mode frequencies and gravitational perturbations of spinning black holes in modified gravity through METRICS: The dynamical Chern-Simons gravity case,” (2025), [arXiv:2503.11759 \[gr-qc\]](#).
 - [18] D. Li, P. Wagle, Y. Chen, and N. Yunes, “Perturbations of spinning black holes beyond General Relativity: Modified Teukolsky equation,” (2022), [arXiv:2206.10652 \[gr-qc\]](#).
 - [19] A. Hussain and A. Zimmerman, “An approach to computing spectral shifts for black holes beyond Kerr,” (2022), [arXiv:2206.10653 \[gr-qc\]](#).
 - [20] P. A. Cano, K. Fransen, T. Hertog, and S. Maenaut, “Universal Teukolsky equations and black hole perturbations in higher-derivative gravity,” *Phys. Rev. D* **108**, 024040 (2023), [arXiv:2304.02663 \[gr-qc\]](#).
 - [21] P. Wagle, D. Li, Y. Chen, and N. Yunes, “Perturbations of spinning black holes in dynamical Chern-Simons gravity: Slow rotation equations,” *Phys. Rev. D* **109**, 104029 (2024), [arXiv:2311.07706 \[gr-qc\]](#).
 - [22] P. A. Cano, K. Fransen, T. Hertog, and S. Maenaut, “Quasinormal modes of rotating black holes in higher-derivative gravity,” (2023), [arXiv:2307.07431 \[gr-qc\]](#).
 - [23] D. Li, P. Wagle, Y. Chen, and N. Yunes, “Perturbations of spinning black holes in dynamical Chern-Simons gravity: Slow rotation quasinormal modes,” (2025), [arXiv:2503.15606 \[gr-qc\]](#).
 - [24] P. A. Cano and A. Ruipérez, “Leading higher-derivative corrections to Kerr geometry,” *Journal of High Energy Physics* **2019**, 189 (2019), [arXiv:1901.01315](#).
 - [25] S. Alexander and N. Yunes, “Chern-Simons Modified General Relativity,” *Phys. Rept.* **480**, 1–55 (2009), [arXiv:0907.2562 \[hep-th\]](#).
 - [26] R. Kallosh and A. Linde, “Dilaton-axion inflation with PBHs and GWs,” *JCAP* **08**, 037 (2022), [arXiv:2203.10437 \[hep-th\]](#).
 - [27] S. H. S. Alexander and S. J. Gates, Jr., “Can the string scale be related to the cosmic baryon asymmetry?” *JCAP* **0606**, 018 (2006), [arXiv:hep-th/0409014 \[hep-th\]](#).
 - [28] J. L. Ripley and F. Pretorius, “Gravitational collapse in Einstein dilaton-Gauss-Bonnet gravity,” *Class. Quant. Grav.* **36**, 134001 (2019), [arXiv:1903.07543 \[gr-qc\]](#).
 - [29] S. Maenaut, G. Carullo, P. A. Cano, A. Liu, V. Cardoso, T. Hertog, and T. G. F. Li, “Ringdown Analysis of Rotating Black Holes in Effective Field Theory Extensions of General Relativity,” (2024), [arXiv:2411.17893 \[gr-qc\]](#).
 - [30] R. D. Blandford and R. L. Znajek, “Electromagnetic extractions of energy from Kerr black holes,” *Mon. Not. Roy. Astron. Soc.* **179**, 433–456 (1977).
 - [31] W. Israel, “Event horizons in static electrovac space-times,” *Commun. Math. Phys.* **8**, 245–260 (1968).
 - [32] D. Li, A. Hussain, P. Wagle, Y. Chen, N. Yunes, and A. Zimmerman, “Isospectrality breaking in the Teukolsky formalism,” *Phys. Rev. D* **109**, 104026 (2024), [arXiv:2310.06033 \[gr-qc\]](#).
 - [33] P. A. Cano and M. David, “Isospectrality in Effective Field Theory Extensions of General Relativity,” (2024), [arXiv:2407.12080 \[hep-th\]](#).
 - [34] S. Tahura and K. Yagi, “Parameterized Post-Einsteinian Gravitational Waveforms in Various Modified Theories of Gravity,” *Phys. Rev. D* **98**, 084042 (2018), [Erratum: *Phys. Rev. D* **101**, 109902 (2020)], [arXiv:1809.00259 \[gr-qc\]](#).
 - [35] R. Abbott *et al.* (LIGO Scientific, Virgo), “GWTC-2: Compact Binary Coalescences Observed by LIGO and Virgo During the First Half of the Third Observing Run,” (2020), [arXiv:2010.14527 \[gr-qc\]](#).
 - [36] M. Isi, M. Giesler, W. M. Farr, M. A. Scheel, and S. A. Teukolsky, “Testing the no-hair theorem with GW150914,” *Phys. Rev. Lett.* **123**, 111102 (2019), [arXiv:1905.00869 \[gr-qc\]](#).
 - [37] M. Isi and W. M. Farr, “Comment on “Analysis of Ringdown Overtones in GW150914”,” *Phys. Rev. Lett.* **131**, 169001 (2023), [arXiv:2310.13869 \[astro-ph.HE\]](#).
 - [38] G. Carullo, W. Del Pozzo, and J. Veitch, “**pyRing**: a time-domain ringdown analysis python package,” [git.ligo.org/lscsoft/pyring](#) (2023).
 - [39] G. Carullo *et al.*, “Empirical tests of the black hole no-hair conjecture using gravitational-wave observations,” *Phys. Rev. D* **98**, 104020 (2018), [arXiv:1805.04760 \[gr-qc\]](#).
 - [40] G. Carullo, G. Riemenschneider, K. W. Tsang, A. Nagar, and W. Del Pozzo, “GW150914 peak frequency: a novel consistency test of strong-field General Relativity,” *Class. Quant. Grav.* **36**, 105009 (2019), [arXiv:1811.08744 \[gr-qc\]](#).
 - [41] G. Carullo, W. Del Pozzo, and J. Veitch, “Observational Black Hole Spectroscopy: A time-domain multimode analysis of GW150914,” *Phys. Rev. D* **99**, 123029 (2019), [Erratum: *Phys. Rev. D* **100**, 089903 (2019)], [arXiv:1902.07527 \[gr-qc\]](#).
 - [42] M. H.-Y. Cheung *et al.*, “Nonlinear Effects in Black Hole Ringdown,” *Phys. Rev. Lett.* **130**, 081401 (2023), [arXiv:2208.07374 \[gr-qc\]](#).
 - [43] K. Mitman *et al.*, “Nonlinearities in Black Hole Ringdowns,” *Phys. Rev. Lett.* **130**, 081402 (2023), [arXiv:2208.07380 \[gr-qc\]](#).
 - [44] P. A. R. Ade *et al.* (Planck), “Planck 2015 results. XIII. Cosmological parameters,” *Astron. Astrophys.* **594**, A13 (2016), [arXiv:1502.01589 \[astro-ph.CO\]](#).
 - [45] H. O. Silva, A. Ghosh, and A. Buonanno, “Black-hole ringdown as a probe of higher-curvature gravity theories,” *Phys. Rev. D* **107**, 044030 (2023), [arXiv:2205.05132 \[gr-qc\]](#).
 - [46] P. Wagle, A. Saffer, and N. Yunes, “Polarization modes

- of gravitational waves in Quadratic Gravity,” [Phys. Rev. D **100**, 124007 \(2019\)](#), [arXiv:1910.04800 \[gr-qc\]](#).
- [47] M. H.-Y. Cheung, L. W.-H. Poon, A. K.-W. Chung, and T. G. F. Li, “Ringdown spectroscopy of rotating black holes pierced by cosmic strings,” [JCAP **02**, 040 \(2021\)](#), [arXiv:2002.01695 \[gr-qc\]](#).
- [48] B. P. Abbott *et al.* (LIGO Scientific, Virgo), “Properties of the Binary Black Hole Merger GW150914,” [Phys. Rev. Lett. **116**, 241102 \(2016\)](#), [arXiv:1602.03840 \[gr-qc\]](#).